IEEE Access
Multidisciplinary | Rapid Review | Open Access Journal

Received June 17, 2021, accepted July 24, 2021, date of publication July 28, 2021, date of current version August 5, 2021.

Digital Object Identifier 10.1109/ACCESS.2021.3100881

Stochastic Approximation Aided Adaptive Thresholding for Optical Detection in PAM4 Based FSO Transmission

JAE-YOUNG CHOI, JOON-WOO LEE, AND SANG-KOOK HAN, (Senior Member, IEEE)
Department of Electrical and Electronic Engineering, Yonsei University, Seoul 03722, South Korea

Corresponding author: Sang-Kook Han (skhan@yonsei.ac.kr)

This work was supported by Institute of Information & communications Technology Planning & Evaluation (IITP) grant funded by the Korea government (MSIT; Ministry of Science and ICT) (No. 2019-0-00685, Free-space-optical-communication-based vertical mobile network).

ABSTRACT This study proposes an adaptive thresholding optical detection technique using a stochastic approximation (SA) to enhance receiver performance in multi-level pulse amplitude modulation (PAM) based free-space optical (FSO) transmission. When the receiver detects the symbol by fixed threshold decision (FTD) scheme, the detection performance of high order modulation, including PAM4, becomes degraded due to a random fluctuation of the received signal. Owing to the slow varying characteristic of atmospheric turbulence, we used an adaptive linear prediction (ALP) filter to predict the decision threshold of the upcoming frame. The experiment was conducted on various degrees of turbulence channels. A Mach-Zehnder modulator (MZM) based turbulence channel emulator was used to experimentally investigate the turbulence-induced scintillation effect. The experiment results confirmed that the proposed technique yielded improved receiver performance compared to FTD. In the case of considering the amplified spontaneous emission (ASE) noise of erbium-doped fiber amplifier (EDFA), the adaptive threshold decision (ATD) scheme obtained about 3dB gain compared with an even-valued threshold (EVT) decision scheme when the average EDFA input optical power was below −16dBm.

INDEX TERMS Adaptive estimation, erbium-doped fiber amplifier, free-space optical communication, multi-level pulse amplitude modulation, scintillation effect.

I. INTRODUCTION

The 3rd Generation Partnership Project (3GPP) has recently considered the development of a non-terrestrial network (NTN) [1], [2]. The NTN is developing scenarios to provide 5G services using airborne vehicles, such as unmanned aircraft systems. The user equipment is connected to the airborne vehicle via a service link, and the airborne vehicle is connected to the gateway via a feeder link. For the feeder link, free-space optical communication (FSOC) can be adopted for NTN scenarios as a hybrid system because FSOCs have more advantages than radio frequency (RF) communication technology: wide bandwidth, small divergence angle, unlicensed spectrum, high security, and low power requirement [3], [4]. However, when a laser beam propagates through an atmospheric channel between the gateway and airborne vehicles, atmospheric turbulence-induced beam scintillation deteriorates the FSOC system. Atmospheric turbulence is an unpredictable phenomenon that causes random fluctuation of the received light intensity. Atmospheric turbulence is caused by variations in the temperature and pressure of the atmosphere. According to the Kolmogorov energy cascading theory [5], [6], it results in the formation of turbulent cells, known as ''eddies,'' which have different sizes and refractive indices. The eddies act like a lens that focuses and defocuses the incoming beams. As a result, they induce received intensity fluctuation, called scintillation.

An important consideration in establishing a stable free-space optical (FSO) link is mitigating the scintillation effect. Studies have been conducted using spatial light modulators (SLM) or digital micro mirror devices for adaptive optics [7], [8]. Another method involves using saturated optical amplifiers as an efficient and straightforward approach to suppress scintillation [9]–[11]. The results are remarkable; however, only the gain saturation effect on the on-off keying (OOK) format was analyzed. In terms of symbol

The associate editor coordinating the review of this manuscript and approving it for publication was Wei-Wen Hu.

detection from the random fluctuation of the received light intensity, studies have been conducted to estimate the decision threshold on the OOK format [12]–[15]. The optimum decision needs perfect instantaneous channel state information (CSI), unavailable in practical systems. However, quasi instantaneous CSI or channel model can be applied to enhance the receiver performance. Maximum likelihood (ML) symbol-by-symbol detection and ML sequence detection techniques were introduced theoretically. The receiver is assumed to know the channel model instead of instantaneous CSI [12], [13]. Both ML symbol-by-symbol detection and ML sequence detection need the accurate marginal distribution of the turbulence-induced fading. However, it is non-attainable in practice, and the distribution model is also not fixed in the FSO channel. So, the receiver has to gather information on the distribution model adaptively and update the decision threshold criteria. Even if the receiver knows the marginal fading distribution, the ML-based fixed threshold decision (FTD) scheme has to overcome the burst errors [15]. Unlike FTD, adaptive threshold decision (ATD) techniques were introduced [14], [15]. In those schemes, the receiver knows the instantaneous fading state. In [14], it applied a low-pass filter (LPF) to extract the CSI from the optical carrier component. This technique uses the slow varying characteristics of turbulence-induced fading and the DC component of the optical signal. Similarly, applying a DC block or AC coupling of a photodiode (PD) can stabilize symbol detection in binary PAM signals. It centers the eye diagram at one and zero levels [9], [10]. However, the decision threshold in a multi-level PAM signal, such as PAM4, needs to be adaptively tracked using another method. PAM4 has multiple levels, implying that the number of thresholds has to be three, unlike one in a binary PAM signal. Therefore, the CSI cannot be estimated using only the LPF or DC block. In [15], it applied a dynamic decision threshold to improve the receiver performance compared with FTD. The FSO signal is detected frame by frame. The duration of each frame is in the order of sub-millisecond, which is smaller than the channel coherence time. Hence in each detection frame, a decision threshold is provided for signal detection by monitoring the preamble. This technique also uses the slow varying characteristics of turbulence-induced fading. However, it has to consider the frame duration. Since each frame is in the order of sub-millisecond, it stores the sampled data on buffer until it monitors the preamble for detection threshold. This problem can be worse with a high data rate since it has to store the increased sampled data, and it disturbs the real-time implementation in the detection process. In addition, the works above have analyzed only in OOK format and are valid for the same noise statistics on the symbol level.

In this paper, we propose a stochastic approximation (SA) aided adaptive threshold decision technique which contributes to PAM4 detection in the presence of different noise statistics on symbol level and the capability of real-time implementation in FSO systems. Based on the slow varying characteristic of the atmospheric turbulence channel, we used the SA algorithm to predict the decision threshold of upcoming frames. We demonstrated that the proposed technique is valid for multi-level modulation signals, e.g., PAM4, which requires a more precise threshold than OOK in FSOC. The experiment was conducted on various degrees of turbulence channels. A Mach-Zehnder modulator (MZM) based turbulence channel emulator was used in experiments to emulate the turbulence-induced scintillation effect. The experimental results confirmed that the proposed technique, compared with FTD, improves the receiver performance. Also, the adaptive threshold decision (ATD) scheme obtained about 3dB gain compared with the even-valued threshold (EVT) scheme when the average erbium-doped fiber amplifier (EDFA) input optical power below −16dBm.

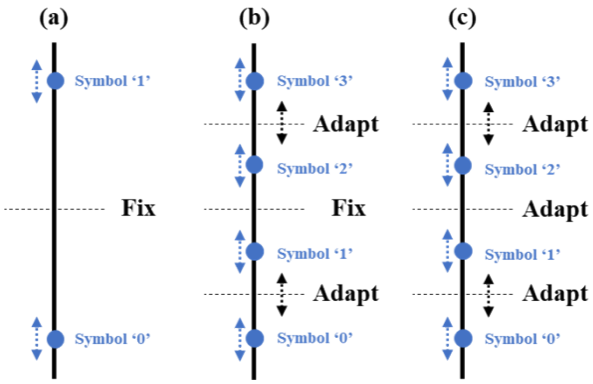

FIGURE 1. Decision threshold in IM/DD-based FSOC systems. (a) Binary PAM case with thermal noise. (b) Multi-level PAM case with thermal noise. (c) Multi-level PAM case with signal-to-ASE beating noise.

II. OPERATION PRINCIPLE

Fig. 1 illustrates the decision threshold in IM/DD-based FSO systems. The response of intensity fluctuation in turbulence is relatively slow compared with that of the data rate with a cutoff frequency of 1 kHz. For this reason, there is a variation in time about the optimal threshold, causing significant burst errors when a fixed threshold is used. Applying a DC block or AC coupling of PD can stabilize symbol detection in binary PAM signal, implying that FTD can be applied. However, the decision threshold in a PAM4 signal needs to be adaptively tracked using another manner. PAM4 has multiple levels, implying that the number of thresholds has to be three, unlike one in a binary PAM signal. Therefore, the CSI cannot be estimated using an LPF function [14]. Moreover, the optical amplifier is used at the receiver, ASE noise can deteriorate the decision process [16], [17]. The total noise is calculated using the following equation:

$$\sigma^2_{total} = \sigma^2_{Signal\times ASE} + \sigma^2_{ASE\times ASE} + \sigma^2_{Shot} + \sigma^2_{Thermal}, \quad (1)$$

where $\sigma^2_{Signal\times ASE}$ and $\sigma^2_{ASE\times ASE}$ are the signal-to-ASE beating noise and ASE-to-ASE beating noise, respectively. In Fig. 1. (c), $\sigma^2_{Signal\times ASE}$ is proportional to the received signal power; therefore, the decision threshold must be adaptively tracked between each symbol.

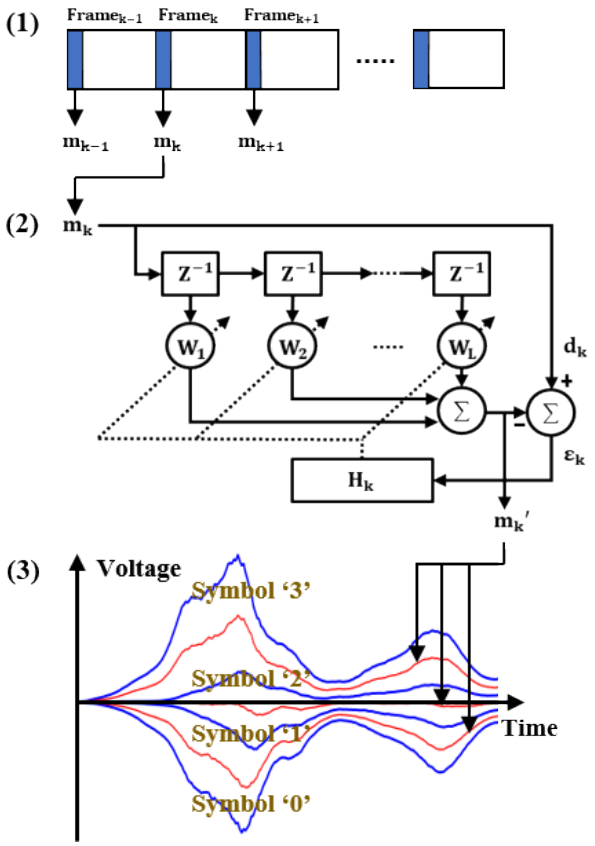

FIGURE 2. Operation principle of the proposed adaptive threshold decision. (1) MLE of the mean obtained from PE. (2) Prediction of upcoming frames using the ALP filter. (3) Adaptive threshold decision process. MLE: maximum likelihood estimate, PE: preamble extraction, ALP: adaptive linear prediction.

Fig. 2 illustrates the operation principle of the proposed ATD. Unlike the binary PAM signal, each decision threshold of the PAM4 signal is adaptively predicted using the SA algorithm. The first step is preamble extraction (PE) for frame synchronization and maximum likelihood estimate (MLE) of mean and variance on power levels of the PAM4 signal in each frame. Frame duration was set to 0.1ms, ten times faster than the cutoff frequency of atmospheric turbulence. The frame duration is the cycle of the threshold update. The preamble comprises 100 symbols for each level, which is 400 symbols for PAM4 levels: "3," "2," "1," and "0" in each frame. The MLE of mean and variance were performed for over 100 symbols, which is 0.8 % overhead in each frame. The preamble size can be optimized, however, it was set to a fixed value to extract the MLE of mean and variance in our study. In the second step, the adaptive linear prediction (ALP) filter is applied to the output of the first step, and it predicts the mean value of each level of the PAM4 signal for upcoming frames. Since the filter is applied to each symbol state, it can be applied for M-ary PAM. However, the system complexity can be increased in proportion to the order M. The ALP filter is a sort of adaptive filter. It is useful in speech and image compression techniques, e.g., linear predictive coding. The purpose of ALP in our study is to use an adaptive filter to predict the future mean value of each PAM4 signal level based on past values. The SA algorithm, also known as the least mean square (LMS) algorithm, was used to solve the coefficient equation of ALP. As the convergence rate of the SA algorithm is relatively slow, it is well matched to the slow varying characteristic of the atmospheric turbulence channel. Moreover, for real-time operation in FSO systems, SA can reduce the burden of coefficient computation. In Fig. 2, the filter input is m_k, the sample mean of the kth frame. The error ε_k is the difference between the filter output m'_k and sample mean of the current frame d_k. The filter output is calculated using the inner product of the weight vector and the filter input vector with tap delays. The number of taps in the ALP filter is set to four. It is the optimal number for tracking the dynamics of intensity fluctuation, which will be discussed later. The SA algorithm is implemented in such a manner as to minimize error. The equation of m_k is

$$m'_k = \vec{H}_k^T \cdot \vec{M}_k, \tag{2}$$

$$\varepsilon_k = d_k - m'_k = d_k - \vec{H}_k^T \cdot \vec{M}_k, \tag{3}$$

where $\vec{H}_k^T = [w_{1,k}, w_{2,k}, \cdots, w_{L,k}]$ is the weight vector and $\vec{M}_k^T = [m_{k-1}, m_{k-2}, \cdots, m_{k-L}]$ is the filter input vector with tap delays of 1 to L. ε_k has to be minimized, and it can be performed by finding the minimum mean square error (MSE). By updating the weight vector with the gradient of MSE ∇_k, the filter can probe the minimum MSE.

$$\vec{H}_{k+1} = \vec{H}_k + \mu \cdot (-\nabla_k), \tag{4}$$

where μ is the convergence rate or learning rate, which determines how fast the filter converges the output. The convergence rate is adjusted with the average received optical power and degrees of turbulence channels in our work. Instead of calculating the gradient of MSE using the input vector statistics, the SA algorithm uses ε_k^2 as an estimate of MSE:

$$\nabla_k = -2 \cdot \varepsilon_k \cdot \vec{M}_k. \tag{5}$$

Therefore, the intensity fluctuation of upcoming frames can be predicted using the sample mean of the past frames with length L. On the other hand, we have applied a moving average filter to obtain exact sample variance. In the last step, the ATD is applied to upcoming frames using the pseudo-optimal threshold [16], which is defined below:

$$\gamma_{n-1} = \frac{m_{n\_level}\sigma_{n-1\_level} + m_{n-1\_level}\sigma_{n\_level}}{\sigma_{n\_level} + \sigma_{n-1\_level}}. \tag{6}$$

The threshold in FTD is determined by averaging the sample means over the long-term FSO channel.

III. EXPERIMENTAL SETUP

The performance of the proposed technique was experimentally verified for different states of the turbulence channel. As shown in Fig. 3, the MZM (JDS IOAP-MOD9140-B-B-O-AA1) based turbulence channel emulator is used. The realization of intensity fluctuation in turbulence is modeled

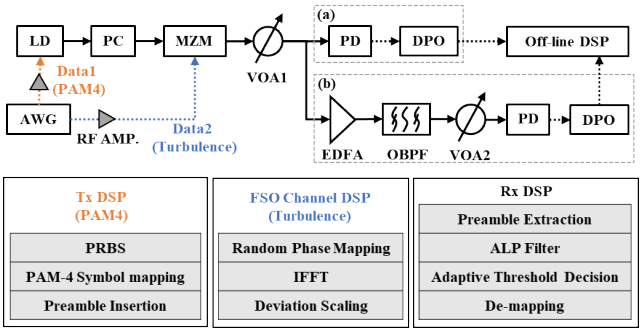

FIGURE 3. Experimental setup and DSP block diagram. (a) Experiment without EDFA. (b) Experiment with EDFA. AWG: arbitrary waveform generator, RF AMP: RF amplifier, LD: laser diode, PC: polarization controller, VOA: variable optical attenuator, OBPF: optical band-pass filter, DPO: digital-processing oscilloscope, DSP: digital signal processing.

on the Kolmogorov power-law spectrum and Taylor frozen hypotheses [18]. The turbulence data are realized by the values of the turbulence spectrum, which undergo random phase mapping, inverse fast Fourier transform (IFFT), and deviation scaling. The power spectral density (PSD) of log-amplitude fluctuation is mathematically modeled as a function of the altitude.

$$W_A(f) = 0.528\pi^2 k^2 \int_0^L dz C_n^2(z) \times \int_{\frac{2\pi f}{v(z)}}^{\infty} [(\kappa v(z))^2 - (2\pi f)^2]^{-1/2} \ldots \kappa^{-8/3} \sin^2\left(\frac{\kappa^2 \gamma z}{2k}\right) F(\gamma\kappa) d\kappa, \quad (7)$$

where k is the optical wave number; L is the propagation distance; z is the altitude; $C_n^2(z)$ is the refractive-index structure parameter, obtained from the Hufnagel-valley model; $v(z)$ is the wind speed, obtained from the Bufton wind model; κ is the spatial wavenumber; γ is the propagation parameter, one for plane waves; $F(\gamma\kappa)$ is the aperture filter function, which is $[2J_1(\gamma\kappa D/2)/(\gamma\kappa D/2)]^2$ for a circular aperture with diameter D; and J_1 is the first kind Bessel function of order one. D was set to 0.05 m. The wavelength and propagation (vertical) distance were 1550 nm and 20 km, respectively. By setting the above parameters, we can derive the shape of the PSD. $C_n^2(z)$ represents the strength of the turbulence as a function of altitude; The strength of the turbulence near the ground is the dominant term of the vertical FSO channel. In this study, we changed the ground turbulence strength to obtain different PSDs. The ground turbulence strengths are $8 \times 10^{-13} m^{-2/3}$, $5 \times 10^{-12} m^{-2/3}$, and $8 \times 10^{-12} m^{-2/3}$. The degree of the scintillation effect is represented in terms of scintillation index (SI) σ_I^2, which is the variance of the intensity fluctuations for the received optical signal. SI is represented by [3]

$$\sigma_I^2 = \frac{\langle I^2 \rangle}{\langle I \rangle^2} - 1, \quad (8)$$

where I is the signal intensity and $\langle \cdot \rangle$ is the ensemble average.

The outputs of the ground turbulence strengths are matched to σ_I^2 of 0.0690, 0.2026, and 0.3045, respectively. In our experiment, only the scintillation effect is emulated through the MZM. The probability density function (pdf) model of the pointing errors (PEs) is not considered in our work under the assumption that a proper pointing, acquisition, and tracking (PAT) function is working. PAT mechanisms in FSOC systems may avoid PEs by continuously measuring the received signal power and Strehl ratio, and adjusting correction elements, such as gimbals, mirrors, or adaptive optics. In the FSO systems, the link between transmitter and receiver has various parameters, such as various degrees of scintillation effect, link distance, link direction, etc. Therefore, the systems may or may not require optical amplifiers, and link margins can be changed in various situations. In our study, we analyzed the performance of the proposed technique under various degrees of turbulence with and without an optical amplifier. The experiments were conducted based on two schemes, as shown in Fig. 3 (a) and (b). PAM4 data was generated by the AWG (TEKTRONIX AWG 70002A) and directly modulated using DFB-LD (Gooch & Housego E0059439) of 1550 nm wavelength. For proof-of-concept experiments, the PAM4 data rate was set to 250 Mbps. It is because our DPO (TEKTRONIX MSO71604C) record length is limited, and the duration of turbulence realization is 0.1 s. In scheme (a), the pre-optical amplifier was not added to determine the proposed ATD and FTD performance. VOA1 was varied to change the average received optical power (ROP) in PD (new focus 1544B). The average received optical power is set at a range of −13 to −5dBm. In scheme (b), the EDFA (LiComm OFA-WCB-15AG) was added to determine different noise statistics on power levels of multi-level signals. VOA1, which monitors the average EDFA input optical power in this structure, varies from −21 to −9dBm. Since the operating range of our EDFA input power is from −26dBm to −8.93dBm, we set the range of the average EDFA input power from -21dBm to −9dBm. The bit-error-rate (BER) was measured on the above range, and the average input power in PD is -3dBm in all points. The BER performance was obtained after the digital signal processing (DSP) went offline. Fig. 4 (a) shows the FSO channel emulation result using the MZM-based turbulence emulator. The results were obtained from DPO. Fig. 4. (b) shows that two different turbulence channel realizations follow lognormal distributions, where ground turbulence strengths are $8 \times 10^{-13} m^{-2/3}$ and $8 \times 10^{-12} m^{-2/3}$. The SI becomes large with ground turbulence strength, and the SI is 0.069 and 0.3045, respectively.

Fig. 4 (c) and (d) show the intensity fluctuation and eye pattern for average EDFA input power values of −21 and −9dBm, respectively. From the eye pattern shown in Fig. 4 (c), ATD is necessary for the small average EDFA input power. If the FTD is used for the small average EDFA input power, it will make burst errors because the EDFA output power fluctuates. However, the eye pattern in Fig. 4. (d) shows that FTD can be applied. When the

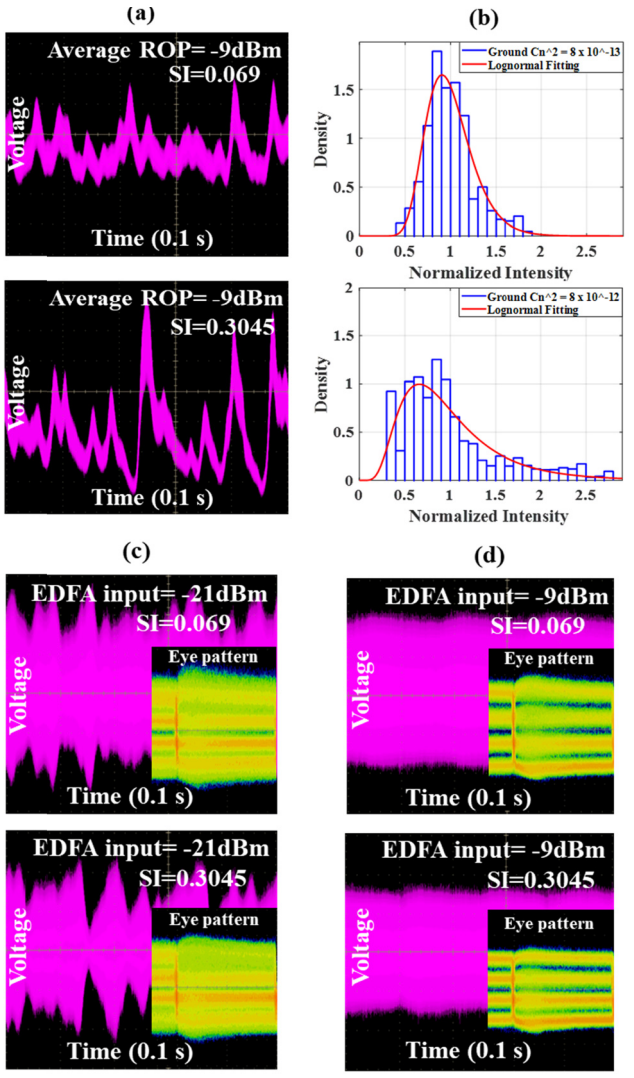

FIGURE 4. Turbulence emulation results. (a) DC-coupled signal without EDFA. (b) Probability density of normalized intensity without EDFA. (c) and (d) Intensity fluctuation and eye pattern of average EDFA input power values of −21 and −9dBm, respectively.

average EDFA input power is high enough, the intensity fluctuation is equalized by the gain saturation of the EDFA. When the average EDFA input power is small, the gain is nearly constant. So, the output of the EDFA has the same gain. However, when the average EDFA input power is large, the gain is non-constant. It means that the high-intensity point has a small gain and the low-intensity point is vice versa.

IV. RESULTS AND DISCUSSION

Before analyzing the performance of the proposed technique, the optimization of tap numbers is required to implement the SA algorithm. Fig. 5 shows the BER performance, which varies with the number of taps. The experimental data, which optimize tap numbers, are obtained at an average received optical power of −13dBm in the absence of EDFA and an average EDFA input optical power of −21dBm in the presence of EDFA. The BER performance is the lowest when the

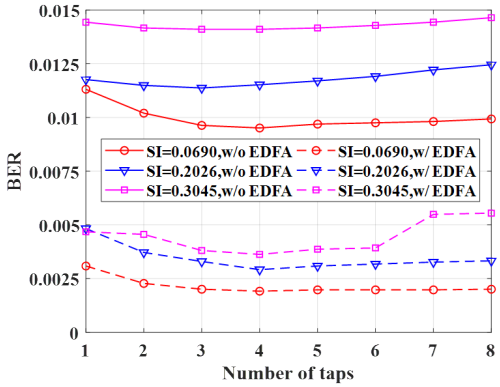

FIGURE 5. BER performances for a different number of taps.

tap number is 4, considering various scintillation effects. The variation of BER is marginal, especially at SI = 0.0690 and SI = 0.2026 in the presence of EDFA. The BER performance will not be marginal with the tap number if the variation of the channel state is dramatic. However, the cutoff frequency of intensity fluctuation is about 1kHz, and the updating cycle of a tap we used is 0.1ms. Considering updating cycle of a tap is 0.1ms, it shows that 0.4ms (4 taps) are required to implement the SA algorithm.

Before comparing the performance with FTD, we validated the proposed ATD. Based on Fig. 2, the MLE of the mean obtained from the preamble is used to predict upcoming frames in our study. Furthermore, considering that the intensity fluctuation is in a quasi-stationary state compared with the data rate, the MLE of the mean obtained from the preamble can be used for CSI. Therefore, we named the ATD using the MLE of mean obtained from the past preamble data as PA-ATD and the ATD using the MLE of mean obtained from the present preamble data as PR-ATD. In Fig. 6 (a) and (b), the BER performance of the proposed ATD is better than that of PA-ATD and PR-ATD. However, there is a slight difference between PA-ATD and PR-ATD owing to the accuracy of the CSI. The result shows that the SA algorithm used in the proposed ATD tracks intensity fluctuation using the sample mean of the past frames. Fig. 6 (c) and (d) illustrate the output of mean tracking when the SI is 0.0690.

The red line shows that it adaptively tracks the dynamics of intensity fluctuation and smooths the intensity fluctuation, including noisy signal. As a result, we can conclude that the proposed ATD helped predict the CSI, which is well matched to the slow varying characteristic of the atmospheric turbulence.

Fig. 7 shows the BER performance of the proposed ATD, proposed EVT, and FTD in the absence of EDFA. The threshold of the proposed ATD is calculated based on the pseudo-optimal threshold, and the proposed EVT is calculated by dividing the tracked mean value of the adjacent symbol by two. The FTD is decided by averaging the sample means over the long-term intensity fluctuation. The received optical power used in Fig. 7 is the average value over

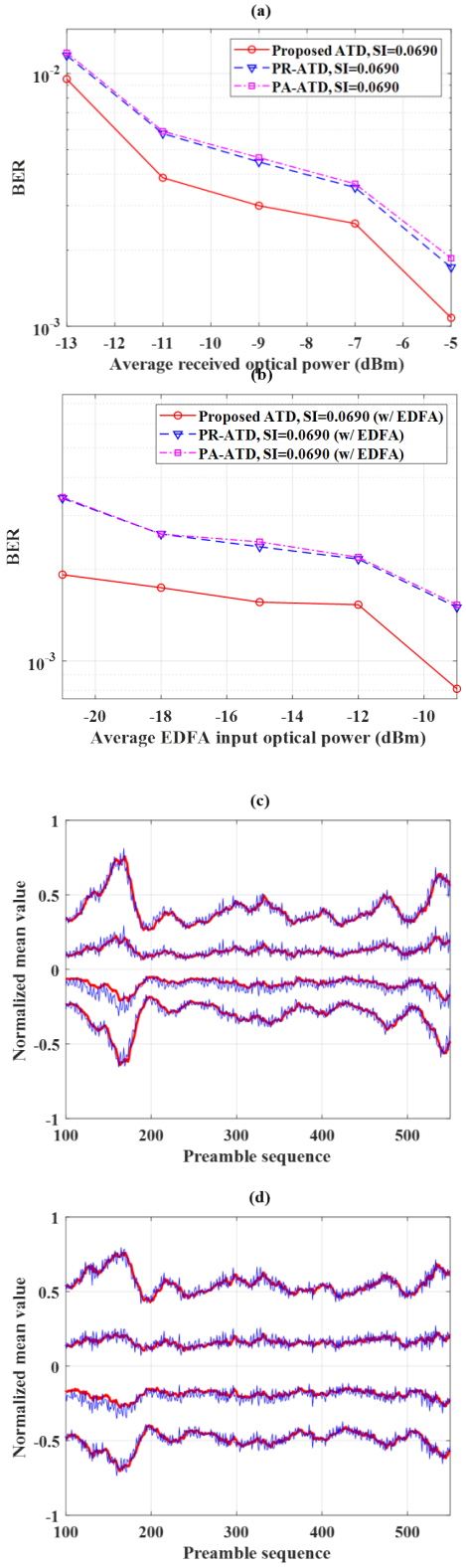

FIGURE 6. (a) Measured BER performance of the proposed ATD, PA-ATD, and PR-ATD in the absence of EDFA. (b) BER performance in the presence of EDFA. (c) Output of mean tracking in the absence of EDFA (the blue line is the MLE of mean, and the red line is the output of the ALP filter, which is used in the proposed ATD). (d) Output of mean tracking in the presence of EDFA.

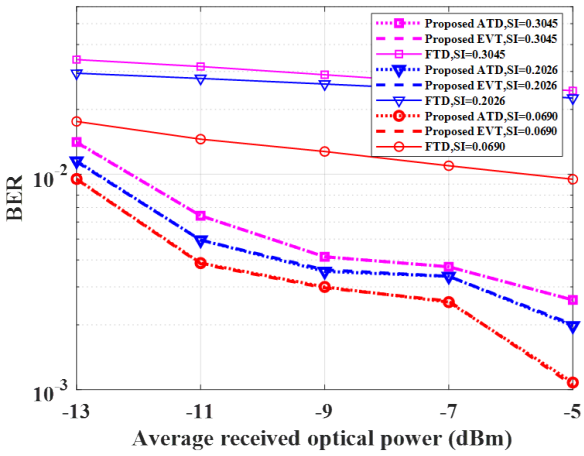

FIGURE 7. BER performance of the proposed ATD, proposed EVT, and FTD without EDFA.

long-term intensity fluctuation. Fig. 7 includes the various scintillation effects of which the SI is 0.3045, 0.2026, and 0.0690. The result shows that the proposed ATD outperforms the FTD without EDFA. However, the proposed ATD and EVT exhibit similar performance. Since the channel does not consist of signal-dependent noise, e.g., signal-to-ASE beating noise. Fig. 8 shows the BER performance of the proposed ATD, proposed EVT, and FTD with EDFA. Unlike the performance without EDFA, the BER performance difference of FTD and the proposed ATD becomes smaller when the EDFA input optical power is high. It is because the EDFA operates in the gain saturation region at high input power. When the average EDFA input power is applied in the gain saturation region, the intensity fluctuation is suppressed (Fig. 4). When the average EDFA input power is -21dBm, the signal power is amplified by EDFA gain, but the intensity fluctuation is not suppressed. Therefore, the result of the gain saturation effect can be seen in Fig. 8 (c), where SI is 0.0690. When the SI is 0.0690, the intensity fluctuation is small; therefore, the performance difference between the FTD and proposed ATD reduces when the average EDFA input power is high. However, the intensity fluctuation in SI $= 0.2026$ and 0.3045 is more significant than that in SI $=$ 0.0690, which means that the intensity fluctuation is not fully equalized when the EDFA input power is high. Therefore, the performance difference between the FTD and proposed ATD does not reduce with increasing EDFA input power. The performance of the proposed ATD obtained about 3dB gain compared with the proposed EVT when the average EDFA input optical power is below -16dBm. Considering that the EDFA gain is high when the input power is low, more ASE is generated. The ASE causes signal-to-ASE beating noise, which is a sort of signal-dependent noise. The beating noise is dependent mainly on the optical amplifier gain and PAM4 symbol level [16]. Fig. 8 (d) shows the ASE beating noise effect on the PAM4 symbol. Unlike the

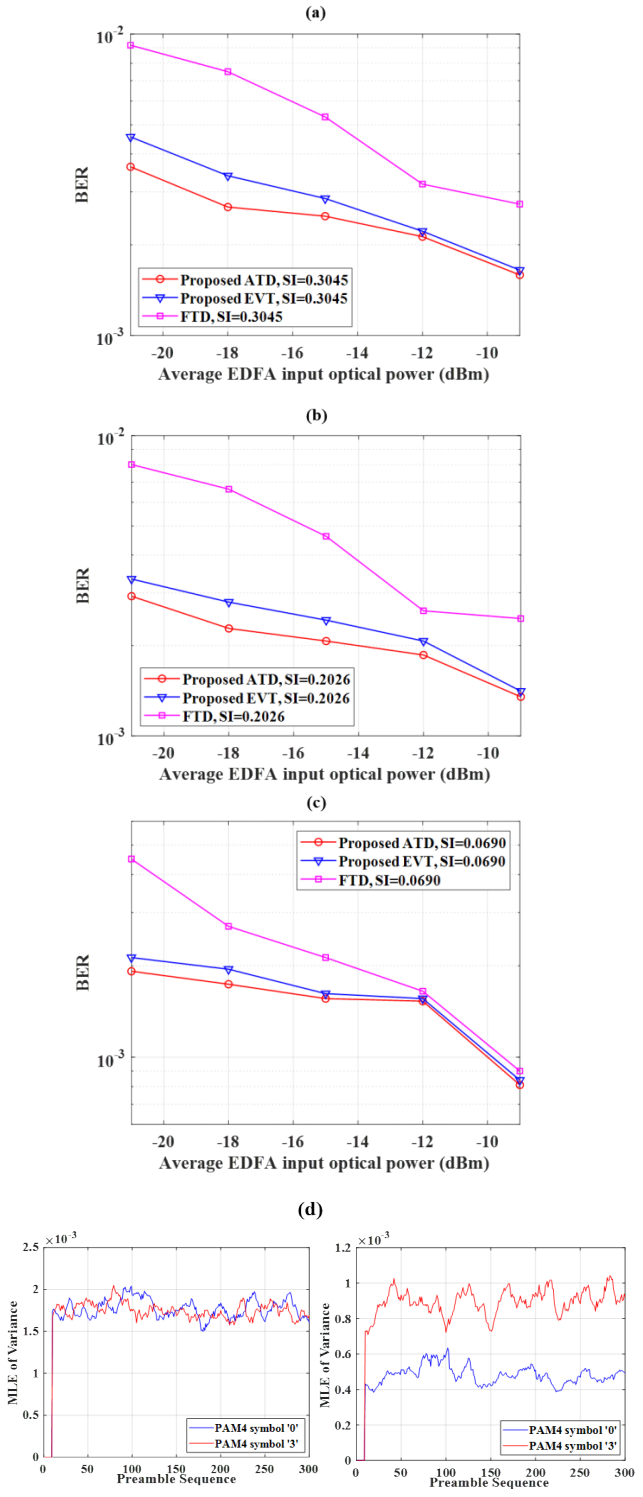

FIGURE 8. BER performance of the proposed ATD, proposed EVT, and FTD with EDFA. (a), (b), and (c) BER performance of SI = 0.3045, 0.2026, and 0.0690, respectively. (d) Left: MLE of variance without EDFA (average received optical power: −13dBm). Right: MLE of variance with EDFA (average EDFA input optical power: −21dBm).

MLE of variance without EDFA, the MLE of variance, when the average EDFA input power is -21dBm, differs between PAM4 symbols "3" and "0." In relay-based all-optical FSO system, multiple relays would increase ASE beating noise effect. So, the proposed ATD can give more precise decision criteria using the adaptive threshold decision process, which considers the different noise statistics on power levels of PAM signals [19]. In our study, we directly modulated the PAM4 signal using DFB-LD. When an external modulator modulates the PAM4 signal, the extinction ratio between each PAM4 symbol level becomes larger. As a result, the overall performance would be better; however, the MLE of variance would have more differences than our experiment results. Consequently, the proposed ATD has enhanced the receiver performance using the SA algorithm in PAM4 FSO transmission. Considering that the multi-level modulation would be in demand for future FSO technology, we believe that the proposed technique would be helpful in multi-level PAM signal detection for IM/DD-based FSO communication.

V. CONCLUSION

In summary, the adaptive threshold decision technique was proposed to enhance receiver performance using the SA algorithm in PAM4 FSO transmission. The experiment was conducted using an MZM-based turbulence channel emulator at various turbulence strengths. According to the experimental results, the proposed ATD adaptively tracked the dynamics of intensity fluctuation and smoothed the intensity fluctuation, including the noisy signal. Experimental results demonstrated that the proposed ATD had better transmission performance than FTD. In the presence of signal-to-ASE beating noise, the performance of the proposed ATD was better than that of the proposed EVT. With this technique, PAM4 detection becomes available in various atmospheric turbulence channels, even in different noise statistics on the power levels of multi-level signals. Considering that the ALP filter predicts the decision threshold of the multi-level signals for upcoming frames, the proposed technique has the capability of real-time implementation in FSO transmission.

REFERENCES

[1] A. Anttonen, P. Ruuska, and M. Kiviranta, "3GPP nonterrestrial networks: A concise review and look ahead," VTT Tech. Res. Centre Finland, Espoo, Finland, Res. Rep. VTT-R-00079-19.
[2] A. Ghosh, A. Maeder, M. Baker, and D. Chandramouli, "5G evolution: A view on 5G cellular technology beyond 3GPP release 15," *IEEE Access*, vol. 7, pp. 127639–127651, 2019.
[3] H. Kaushal and G. Kaddoum, "Optical communication in space: Challenges and mitigation techniques," *IEEE Commun. Surveys Tuts.*, vol. 19, no. 1, pp. 57–96, 1st Quart., 2017.
[4] M. A. Khalighi and M. Uysal, "Survey on free space optical communication: A communication theory perspective," *IEEE Commun. Surveys Tuts.*, vol. 16, no. 4, pp. 2231–2258, Nov. 2014.
[5] L. C. Andrews and R. L. Phillips, *Laser Beam Propagation Through Random Media*, 2nd ed. Bellingham, WA, USA: SPIE, 2005.
[6] L. C. Andrews, R. L. Phillips, and C. Y. Hopen, *Laser Beam Scintillation With Applications*. Bellingham, WA, USA: SPIE, 2001.
[7] Y. Ren, G. Xie, H. Huang, C. Bao, Y. Yan, N. Ahmed, M. P. J. Lavery, B. I. Erkmen, S. Dolinar, M. Tur, M. A. Neifeld, M. J. Padgett, R. W. Boyd, J. H. Shapiro, and A. E. Willner, "Adaptive optics compensation of multiple orbital angular momentum beams propagating through emulated atmospheric turbulence," *Opt. Lett.*, vol. 39, no. 10, pp. 2845–2848, 2014.
[8] M. N. Horenstein, S. Pappas, A. Fishov, and T. G. Bifano, "Electrostatic micromirrors for subaperturing in an adaptive optics system," *J. Electrostatics*, vol. 54, nos. 3–4, pp. 321–332, Mar. 2002.

[9] M. Abtahi, P. Lemieux, W. Mathlouthi, and L. A. Rusch, "Suppression of turbulence-induced scintillation in free-space optical communication systems using saturated optical amplifiers," *J. Lightw. Technol.*, vol. 24, no. 12, pp. 4966–4973, Dec. 2006.
[10] M. Abtahi and L. A. Rusch, "Mitigating of scintillation noise in FSO communication links using saturated optical amplifiers," in *Proc. IEEE Mil. Comm. Conf.*, Monterey, CA, USA, Oct. 2006, pp. 1–5.
[11] Y.-Q. Hong, W.-H. Shin, and S.-K. Han, "Enhancement of SOA-based scintillation mitigation by PS-OOK transmission in FSO communication," *IEEE Photon. J.*, vol. 12, no. 4, pp. 1–10, Aug. 2020.
[12] X. Zhu and J. M. Kahn, "Free-space optical communication through atmospheric turbulence channels," *IEEE Trans. Commun.*, vol. 50, no. 8, pp. 1293–1300, Aug. 2002.
[13] W.-H. Shin, J.-Y. Choi, and S.-K. Han, "Fixed threshold on-off keying differential detection for satellite optical communications," *Opt. Exp.*, vol. 27, no. 2, p. 1590, Jan. 2019.
[14] S. Ding, J. Zhang, and A. Dang, "Adaptive threshold decision for on-off keying transmission systems in atmospheric turbulence," *Opt. Exp.*, vol. 25, no. 20, pp. 24425–24436, 2017.
[15] Z. Wang, W. Zhong, and C. Yu, "Performance improvement of OOK free-space optical communication systems by coherent detection and dynamic decision threshold in atmospheric turbulence conditions," *IEEE Photon. Tech. Lett.*, vol. 24, no. 22, pp. 2035–2037, Nov. 15, 2012.
[16] S. B. Alexander, *Optical Communication Receiver Design*. London, U.K.: SPIE, 1997, pp. 253–282.
[17] P. Saxena, A. Mathur, and M. R. Bhatnagar, "BER performance of an optically pre-amplified FSO system under turbulence and pointing errors with ASE noise," *J. Opt. Commun. Netw.*, vol. 9, no. 6, pp. 498–510, 2017.
[18] H. Shen, L. Yu, and C. Fan, "Temporal spectrum of atmospheric scintillation and the effects of aperture averaging and time averaging," *Opt. Commun.*, vol. 330, pp. 160–164, Nov. 2014.
[19] N. A. M. Nor, Z. Ghassemlooy, J. Bohata, P. Saxena, M. Komanec, S. Zvanovec, M. R. Bhatnagar, and M.-A. Khalighi, "Experimental investigation of all-optical relay-assisted 10 Gb/s FSO link over the atmospheric turbulence channel," *J. Lightw. Technol.*, vol. 35, no. 1, pp. 45–53, Jan. 1, 2017.

JAE-YOUNG CHOI received the B.S. degree in electrical and electronic engineering from Yonsei University, Seoul, Republic of Korea, in 2017, where he is currently pursuing the Ph.D. degree in electrical and electronic engineering. His current research interests include inter-satellite optical communication, NTN architecture, and free space optical systems.

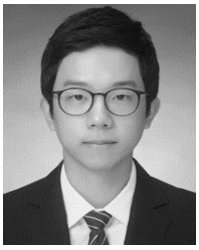

JOON-WOO LEE received the B.S. degree in electrical and electronic engineering from Ajou University, Suwon, Republic of Korea, in 2015. He is currently pursuing the Ph.D. degree in electrical and electronic engineering with Yonsei University. His current research interests include visible-light communication, optical camera communication, and indoor positioning systems.

SANG-KOOK HAN (Senior Member, IEEE) received the B.S. degree in electronic engineering from Yonsei University, Seoul, South Korea, in 1986, and the M.S. and Ph.D. degrees in electrical engineering from the University of Florida, Gainesville, FL, USA, in 1994. From 1994 to 1996, he was with the System IC Laboratory, Hyundai Electronics, where he was involved in the development of optical devices for telecommunications. He is currently a Professor with the Department of Electrical and Electronic Engineering, Yonsei University. His current research interests include optical devices/systems for communications, optical OFDM transmission systems, optical networks, and optical wireless communications, including visible-light communication.